Article:
Stewart, N.J., Sato, T., Takeda, N. et al. (2022) Hyperpolarized 13C MRI as a tool for imaging tissue redox state, oxidative stress, inflammation and cellular metabolism. Antioxidants & Redox Signaling, 36 (1-3). pp. 81-94. ISSN: 1523-0864

https://doi.org/10.1089/ars.2021.0139

ANTIOXIDANTS & REDOX SIGNALING
Volume 00, Number 00, 2021
Mary Ann Liebert, Inc.
DOI: 10.1089/ars.2021.0139

Hyperpolarized ^{13}C Magnetic Resonance Imaging as a Tool for Imaging Tissue Redox State, Oxidative Stress, Inflammation, and Cellular Metabolism

Neil J. Stewart,[1,2] Tatsuyuki Sato,[3–5] Norihiko Takeda,[3] Hiroshi Hirata,[1,i] and Shingo Matsumoto[1,ii]

Abstract

Significance: Magnetic resonance imaging (MRI) with hyperpolarized (HP) ^{13}C-labeled redox-sensitive metabolic tracers can provide noninvasive functional imaging biomarkers, reflecting tissue redox state, oxidative stress, and inflammation, among others. The capability to use endogenous metabolites as ^{13}C-enriched imaging tracers without structural modification makes HP ^{13}C MRI a promising tool to evaluate redox state in patients with various diseases.

Recent Advances: Recent studies have demonstrated the feasibility of *in vivo* metabolic imaging of ^{13}C-labeled tracers polarized by parahydrogen-induced polarization techniques, which offer a cost-effective alternative to the more widely used dissolution dynamic nuclear polarization-based hyperpolarizers.

Critical Issues: Although the fluxes of many metabolic pathways reflect the change in tissue redox state, they are not functionally specific. In the present review, we summarize recent challenges in the development of specific ^{13}C metabolic tracers for biomarkers of redox state, including that for detecting reactive oxygen species.

Future Directions: Applications of HP ^{13}C metabolic MRI to evaluate redox state have only just begun to be investigated. The possibility to gain a comprehensive understanding of the correlations between tissue redox potential and metabolism under different pathological conditions by using HP ^{13}C MRI is promoting its interest in the clinical arena, along with its noninvasive biomarkers to evaluate the extent of disease and treatment response. *Antioxid. Redox Signal.* 00, 000–000.

Keywords: DNP, hyperpolarized ^{13}C MRI, inflammation, oxidative stress, parahydrogen, redox state

Introduction

Over the past several decades, numerous studies have revealed that cellular and tissue redox state shifts from the homeostatic balance in a range of pathological conditions, including cancer, stroke, inflammation, diabetes, and viral infections, among others (14). Changes in redox environment can induce increased oxidative stress and affect gene expression that regulates the energy metabolism of cells. Many enzymes require redox sensitive cofactors such as NAD^+/

[1]Division of Bioengineering & Bioinformatics, Graduate School of Information Science & Technology, Hokkaido University, Sapporo, Japan.
[2]POLARIS, Imaging Sciences, Department of Infection, Immunity and Cardiovascular Disease, University of Sheffield, Sheffield, United Kingdom.
[3]Division of Cardiology and Metabolism Center for Molecular Medicine, Jichi Medical University, Shimotsuke-shi, Japan.
[4]Department of Cardiovascular Medicine, Graduate School of Medicine, The University of Tokyo, Tokyo, Japan.
[5]Japan Society for the Promotion of Science, Tokyo, Japan.
[i]ORCID ID (https://orcid.org/0000-0002-6906-1608).
[ii]ORCID ID (https://orcid.org/0000-0003-2698-0839).

NADH or $FAD/FADH_2$ for their enzymatic activity; as such, the tissue redox state can be estimated by measuring the concentration ratio of a specific redox couple of metabolites (62), whose reversible metabolic reaction is catalyzed by such redox-sensitive enzymes.

The concentration ratio of lactate-to-pyruvate has been traditionally used to estimate the redox potential of cells and tissues. For example, the difference in concentration ratio of the lactate/pyruvate in arterial and coronary vein blood revealed that the redox potential of heart muscle was ~ 20 mV more negative under anoxia compared with under normoxic conditions (24), where the pyruvate-to-lactate metabolic flux is related to the cytosolic $NAD^+/NADH$ couple as a result of the rapid equilibrium of the lactate dehydrogenase activity.

The development of the dissolution dynamic nuclear polarization (d-DNP) hyperpolarization technique, by which the magnetic resonance imaging (MRI) signal obtainable from ^{13}C-labeled metabolic tracers is enhanced by more than 10,000 times, has enabled the realization of noninvasive monitoring of the flux of a particular metabolic reaction in real time (4, 22). Hyperpolarized (HP) ^{13}C-labeled pyruvate—the most widely studied HP ^{13}C MRI tracer to date—is taken up by cells and undergoes the same metabolism as endogenous pyruvate. As such, ^{13}C labeling of pyruvate in the C-1 position allows the study of pyruvate-lactate metabolism (and in turn, the Warburg effect in cancer), whereas labeling in the C-2 position permits further metabolic pathways in the citric acid cycle to be probed.

Metabolic MRI of HP [1-^{13}C] pyruvate has revealed that the conversion rate of pyruvate to lactate depends on the tissue microenvironment in living creatures, including humans (51), and this metabolic conversion efficiency can be used as a noninvasive biomarker of the extent of the disease and its response to treatments (43, 44). More than 60 different ^{13}C tracers for HP ^{13}C MRI studies have already been reported in *in vitro* and *in vivo* preclinical applications (31), some which are specific to tissue redox state. In the present review, we summarize the recent progress in HP ^{13}C MRI techniques, focused on the metabolic tracers that hold most promise for the detection of the redox state *in vivo*.

HP ^{13}C MRI for Redox-Sensitive Metabolic Imaging

^{13}C is a nuclear magnetic resonance (NMR)-sensitive isotope of carbon that has a gyromagnetic ratio $\sim 4\times$ lower than that of ^1H, and around 1.1% natural abundance. Thanks to its extensive chemical shift range (~ 200 ppm, compared with ~ 10 ppm for ^1H), ^{13}C NMR presents an attractive method for interrogation of metabolism *in vivo* (58). Further, detection at the Larmor frequency of ^{13}C yields low background signal and a high contrast. Nevertheless, the sensitivity is relatively poor, and it remains challenging to obtain high-quality spectroscopy or imaging data even after injection of ^{13}C-enriched metabolic probes (8).

Hyperpolarization offers a means to circumvent this sensitivity limitation. By biasing the relative populations of the ground-state nuclear energy levels in the presence of a magnetic field, a four to five order of magnitude boost in the attainable magnetic resonance (MR) signal can be realized. The two most common methods employed for hyperpolarization of ^{13}C nuclei are d-DNP (4) and parahydrogen-induced polarization (PHIP) (7, 56). d-DNP relies on the fact that the electron gyromagnetic ratio is ~ 660 times greater than that of ^1H, which leads to a near-unity polarization under extreme conditions. On cooling a sample mixed with glassing agent and free radicals to ~ 1 K in the presence of a strong magnetic field (several Tesla), microwave irradiation is used to induce polarization transfer from the free electrons to ^{13}C nuclei in the solid state (Fig. 1). The sample is then rapidly dissolved and transported to the MRI system for delivery into the subject.

On the other hand, PHIP utilizes the innate spin order of parahydrogen (a spin isomer of the hydrogen molecule) to induce ^{13}C nuclear polarization by irreversible, direct addition of parahydrogen to the molecule of interest (18) or reversible interaction with an intermediary (1). In the following, we will focus on applications of d-DNP that are pertinent to the assessment of redox state; for further information on the differences between d-DNP and PHIP, and the ^{13}C MRI probes that can be accessed with PHIP, we refer the readers to our recent review article (66).

Laboratory set-up requirements

To establish HP ^{13}C MRI technology in a new laboratory, the following requirements must be met:

(i) Polarization device: A number of commercial and open-source ^{13}C DNP and PHIP (13) polarizer apparatus are available for the production of a wide variety of HP ^{13}C molecules for *in vitro* and preclinical *in vivo* metabolic imaging experiments. At present, only one sterile polarizer approved for clinical HP ^{13}C metabolic MRI exists: the GE Healthcare SpinLab device (5).

(ii) The MR system is capable of multi-nuclear MRI; that is, such that the detection of nuclei other than ^1H is enabled. Multi-nuclear functionality is typically available on high-field NMR systems and most preclinical MRI systems by default, whereas multi-nuclear clinical MRI scanners remain less common, and MR vendor support must be sought to install hardware and software for this purpose.

(iii) MR coils for ^{13}C (or other nuclei of choice): Radiofrequency coils for detection of MR signal at Larmor frequencies other than that of ^1H nuclei are not routinely supplied by MR vendors, and therefore they must be purchased separately or custom built on site.

(iv) Optimal pathway for tracer delivery from polarizer to subject: The polarization of HP ^{13}C molecules tends to decay over the order of tens of seconds, and thus it is usually necessary to situate the polarizer close to the MRI scanner for rapid sample transport and injection, and/or magnetically shield the sample during the transport process (46). In the case of human use, such pathways must be sterile.

Tracer characteristics

In the following section, we review the most common ^{13}C tracers used for metabolic MRI applications. The biochemistry of such imaging tracers is a highly active area of research, and a full review is beyond the scope of this article [we refer the readers to Refs. (32, 66)]. When designing an HP ^{13}C tracer for *in vivo* metabolic MRI applications, it is important to consider the following requirements (61):

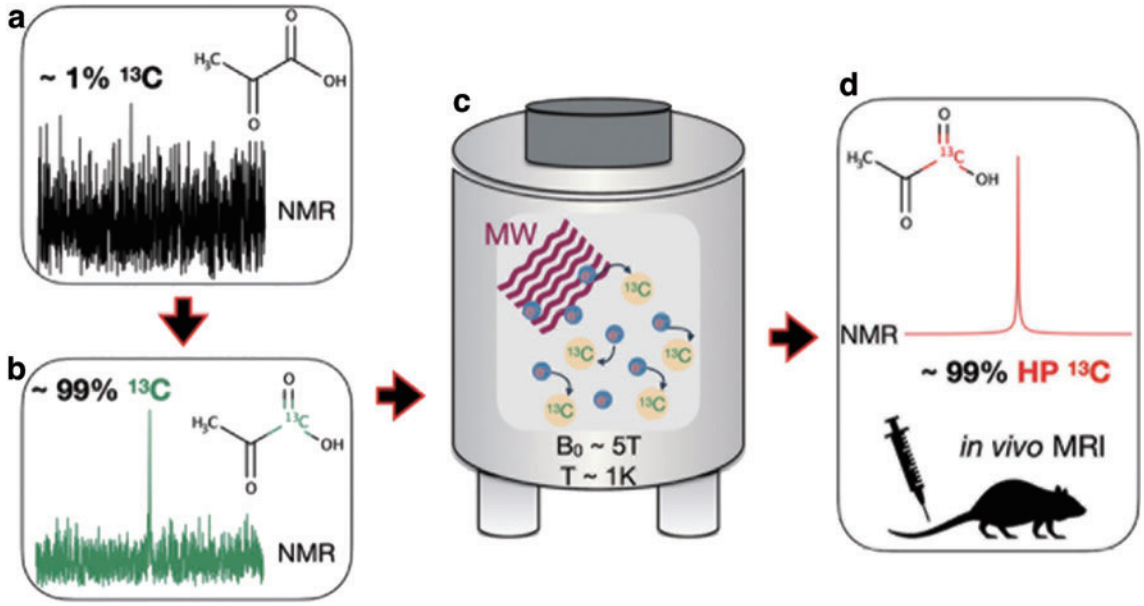

FIG. 1. Overview of the hyperpolarization process, using [1-^{13}C] pyruvate as an example. **(a)** Natural abundance carbon comprises mostly ^{12}C, which is not NMR-detectable. **(b)** Enrichment of the ^{13}C isotope, typically by labeling the ''1'' position as shown, can lead to a detectable NMR signal, though the sensitivity remains low and requires averaging over several acquisitions (often approximately hours) to obtain a reasonable signal-to-noise. **(c)** Hyperpolarization of a ^{13}C-labeled sample by DNP requires placing the sample in a high field magnet at extremely low temperatures, where, in the presence of free radicals, microwave radiation is used to induce ^{13}C nuclear polarization *via* transfer from the free electrons. **(d)** The NMR signal obtainable from the hyperpolarized product molecule is typically enhanced by $\sim 10^{4-5}$ times that of the thermally polarized sample in **(b)**, and it is sufficient for *in vivo* imaging (usually by injection). DNP, dynamic nuclear polarization; NMR, nuclear magnetic resonance. Color images are available online.

(i) Biological safety/compatibility: HP ^{13}C tracers are typically chemically identical to endogenous molecules (aside from ^{13}C-labeling) or are otherwise biologically inert.

(ii) Metabolically active: Many HP ^{13}C tracers exhibit metabolic activity without the requirement of co-factors. (^{13}C-urea is an exception and exhibits no metabolic activity.)

(iii) Chemical shift sensitivity: By virtue of the extensive chemical shift range exhibited by the ^{13}C nucleus, different metabolites exhibit distinct chemical shift values; this critical feature allows selective interrogation of MR signal dynamics to quantify metabolic behavior. Nevertheless, it must be ensured that the chemical shift difference between reactant and product of the metabolic reaction of interest is detectable (ideal case: approximately few parts per million on conventional MRI systems).

(iv) Sufficiently long polarization lifetime: The MR signal enhancement conferred by d-DNP or other hyperpolarization methods is nonpermanent, and the ^{13}C nuclear polarization decays to that of the thermal equilibrium value on a timescale of the spin-lattice relaxation time (T_1); typically, of the order of several seconds and governed by ^{13}C-labeling position, molecular weight, and detection field strength among other factors. For example, the most commonly used HP ^{13}C metabolic imaging probe to date—[1-^{13}C] pyruvate—exhibits a T_1 of around 65 s at 3 T (9). Novel probes must have a sufficient T_1 to ensure detectable signal remains after polarization and delivery to the subject in the MR scanner.

(v) Absorption, distribution, metabolism, and excretion (ADME): The tracer must be delivered to the target organ within the polarization lifetime (iv), and the associated signal should be free of influence (or otherwise decouplable) from that of neighboring tissues. In the HP ^{13}C MRI experiments, it is typical to wait 20–30 s after intravenous injection of HP ^{13}C tracer before MRI scans for the tracer to well distribute into peripheral regions. As most tracers are endogenous and/or involved in metabolic processes, *excretion* is not usually a concern, though it should be considered for new exogenous tracers. HP ^{13}C dynamic NMR/MRI can be used to study ADME properties of new tracers; and importantly, perfusion to the organ of interest is monitored dynamically by using MR spectroscopy before any imaging acquisition to determine the most appropriate acquisition timing.

Acquisition techniques

The most basic acquisition method used to probe metabolic activity with HP ^{13}C tracers is dynamic MR spectroscopy, wherein the MR signal kinetics determines the relative metabolic flux. Spectroscopy provides a global measurement of the metabolic activity within a certain region (*e.g.,* the whole body, or a slice of the anatomy), whereas MR spectroscopic imaging (MRSI) extends this approach to generate distinct images of the MR signal detected from each metabolite. MRSI comprises a class of methods, including chemical shift imaging (22), echo planar spectroscopic imaging (35), and IDEAL spectral decomposition methods (72) (in order of

Table 1. Currently Available ^{13}C Magnetic Resonance Imaging Tracers That Can Be Used to Assess Metabolic Processes, Including Aspects of Redox State

^{13}C MRI Tracer [δ]	*Metabolic Product(s) [δ]*	*Biomarker (ref)*
[1,3-$^{13}C_2$] AcAc [175.0, 210.4]	[1,3-^{13}C] βOHB [180.4–180.6, doublet: 67.3, 65.8]	βOHB/AcAc ratio: to assess mitochondrial redox state (10, 71)
[1-^{13}C] alanine [179]	See [1-^{13}C] pyruvate	Lac/Pyr ratio after conversion from alanine: to assess intracellular redox state (55)
^{13}C bicarbonate ($H^{13}CO_3^-$) [161]	^{13}C carbon dioxide ($^{13}CO_2$) [125]	CO_2/HCO_3^- ratio: to assess tumor pH (19)
[1-^{13}C] DHA [175]	[1-^{13}C] AA [179]	AA/DHA or AA/(AA+DHA) ratio: to assess redox state (6, 28)
[1,4-$^{13}C_2$] fumarate [175]	[1-^{13}C] malate, [4-^{13}C] malate [181.8, 180.6]	HP ^{13}C Malate production: to assess necrotic cell death (20, 67)
[1-^{13}C] pyruvate[a] (Pyr) [173]	[1-^{13}C] lactate (Lac) [185], [1-^{13}C] alanine [178], [1-^{13}C] bicarbonate [162], [1-^{13}C] pyruvate hydrate [181]	Lac/Pyr ratio, reaction rates, for example, k_{PL}: to assess the Warburg effect (34)
^{13}C urea [162.5]	N/A	Urea signal, blood flow *etc.*: to assess perfusion (36)

δ: NMR chemical shift in parts per million; ref: literature reference(s).
[a]Pyruvate can also be ^{13}C-labeled in the 2 position.
βOHB, β-hydroxybutyrate; AA, ascorbic acid; AcAc, acetoacetate; DHA, dehydroascorbic acid; HP, hyperpolarized; MRI, magnetic resonance imaging; NMR, nuclear magnetic resonance.

increasing acquisition efficiency at the expense of spectral information), and it is performed either dynamically, or at a single time-point that is often chosen to coincide with the peak MR signal of the metabolic product of interest (*e.g.*, as predetermined from dynamic MR spectroscopy).

Quantification methods

The MR signal ratios of ^{13}C in different metabolites are commonly used as simplistic yet quantitative biomarkers of metabolic activity (see Table 1 for examples). This approach is effective for analysis of single time-point spectroscopy or imaging data; for example, lactate-to-pyruvate ratio as a marker of the Warburg effect in cancer detection and staging (3). Further quantitative information can be gleaned by acquiring MR spectra dynamically and fitting the time dependence of the MR signals with kinetic models of the chemical exchange process (25). This enables the derivation of parameters such as the forward and backward metabolic reaction rates (*e.g.,* k_{PL} and k_{LP} for pyruvate–lactate conversion), in addition to the spin-lattice relaxation rates; for example, reduced k_{PL} flux post-ablation and chemotherapy in a patient with high-grade prostate cancer as a marker of treatment response (2).

HP ^{13}C MRI Tracers for Imaging Redox State

A nonexhaustive list of ^{13}C metabolic imaging probes that can be polarized by d-DNP is presented in Table 1, along with their associated biomarkers and biomedical uses [for a more comprehensive review, see, *e.g.,* Refs. (31, 66)]. The most widely studied HP ^{13}C metabolic MRI tracer to date is [1-^{13}C] pyruvate; its conversion to HP [1-^{13}C] lactate and other metabolites (including [1-^{13}C] alanine and [1-^{13}C] bicarbonate) are key components of cellular metabolism. In particular, increased glycolytic pyruvate–lactate metabolism is a hallmark of cancer cells (the so-called Warburg effect); as such, the relative production of HP [1-^{13}C] lactate to HP [1-^{13}C] pyruvate provides a sensitive measure of cancer state (Fig. 2a, b). This metabolic information is distinct (downstream), and complementary to that of ^{18}F fluorodeoxyglucose-positron emission tomography (FDG-PET), which is used clinically to probe the first step of the glycolysis metabolic pathway.

Numerous preclinical studies have reported elevated HP [1-^{13}C] lactate flux in a wide range of cancer models (3, 22, 30). In particular, HP [1-^{13}C] pyruvate MRI is well suited to the assessment of new and existing cancer therapies (16, 54, 59, 75), thanks to its high sensitivity, safety, and nonionizing properties. With the advent of sterile, high-throughput d-DNP polarizer systems (5), *in vivo* human studies of HP [1-^{13}C] pyruvate to HP [1-^{13}C] lactate metabolism in prostate (2, 51), pancreatic (68), and breast cancer (21), and the healthy and unhealthy heart (15, 57) and brain (23, 48) have been realized, and clinical trials are underway at several sites across the globe. Though most commonly labeled with ^{13}C in the 1 position, pyruvate can also be ^{13}C-labeled in the 2 position, which enables further interrogation of downstream TCA cycle metabolism (12, 26) that cannot be probed with [1-^{13}C] pyruvate.

Beyond pyruvate, HP [1,4-$^{13}C_2$] fumarate has been developed as a sensitive tracer of cellular necrosis; exogenously delivered fumarate cannot easily permeate into healthy cells, and thus production of HP [1-^{13}C], [4-^{13}C] malate only occurs when the cellular plasma membrane integrity is damaged by necrotic processes (20). This selective HP ^{13}C malate production has been utilized to study necrotic processes in myocardial infarction (47) and diabetic nephropathy (37) among other conditions, and it offers a sensitive means to interrogate response to treatment of tumors (19, 74). HP ^{13}C Bicarbonate ($H^{13}CO_3^-$) and its conversion to ^{13}C carbon dioxide can be used to map pH *in vivo*, for example, its use has been reported in murine tumors (19), ischemic rat hearts (63), and ventilator-induced lung injury (17). [1-^{13}C] Urea is readily polarizable by using d-DNP (4), and, as one of the few probes in common use that exhibits no metabolic activity, it finds application as a probe of perfusion; for example, in imaging of blood flow (70) and assessment of renal function (52). Further, it can be co-polarized with [1-^{13}C] pyruvate for simultaneous assessment of metabolism and perfusion (36).

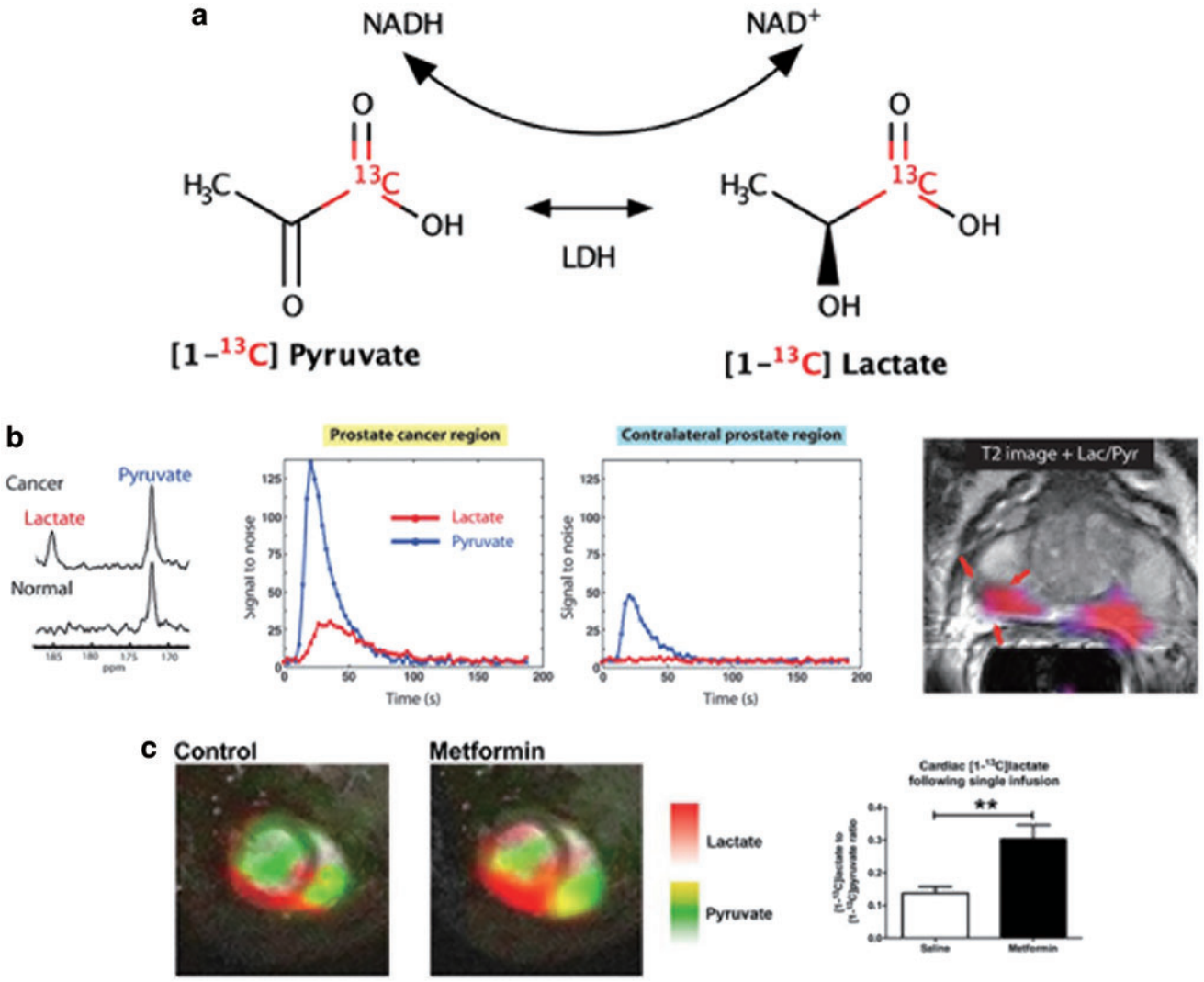

FIG. 2. Assessment of pyruvate–lactate metabolism with HP [1-^{13}C] pyruvate tracer. (a) Schematic of the conversion of HP [1-^{13}C] pyruvate to [1-^{13}C] lactate *via* LDH. **(b)** *Left*: HP ^{13}C MR spectra and pyruvate and lactate peak signal intensities as a function of time in the prostate cancer region and contralateral (healthy) prostate region of a patient with prostate cancer, and *right*: [1-^{13}C] lactate/[1-^{13}C] pyruvate ratio map overlaid on a T_2-weighted anatomical ^{1}H MR image [adapted from Nelson *et al.* (51) with permission from the American Association for the Advancement of Science]. **(c)** Increase in HP [1-^{13}C] lactate signal (localized to the left ventricular myocardium) upon metformin treatment, concordant with an increase in cytosolic redox state [adapted from fig. 2 of Lewis *et al.* (39) with permission from the American Diabetes Association]. $^{**}p < 0.01$. HP, hyperpolarized; LDH, lactate dehydrogenase; MR, magnetic resonance. Color images are available online.

The most studied HP ^{13}C-labeled tracers for assessment of redox state *in vivo* are the reduced and oxidized forms of vitamin C, namely HP [1-^{13}C] dehydroascorbic acid (DHA) and [1-^{13}C] ascorbic acid (AA) (6, 28) (Figs. 3 and 4). Both of these molecules are polarizable to acceptable levels of sensitivity by d-DNP and offer different insights into redox processes; HP [1-^{13}C] AA is sensitive to extracellular reactive oxygen species (ROS), whereas HP [1-^{13}C] DHA reflects intracellular redox state, highlighted by the lack of extracellular oxidation of HP [1-^{13}C] AA and rapid intracellular reduction of HP [1-^{13}C] DHA in murine lymphoma tumors (6) (Fig. 3b). As such, subsequent studies have focused on the application of HP [1-^{13}C] DHA and its reduction to AA, a reaction that can be mediated by glutathione- (GSH) or NADPH-dependent mechanisms (in turn, NADPH-dependent reduction of oxidized glutathione to GSH maintains levels of the latter) (28). For example, after introduction of HP [1-^{13}C] DHA into the healthy rat brain, high levels of HP [1-^{13}C] AA were observed, highlighting the brain's reductive properties (Fig. 4a) (28).

The upregulation of glutathione in cancer cells to counteract oxidative stress has been studied by using HP [1-^{13}C] DHA in transgenic adenocarcinoma of the mouse prostate (TRAMP) tumors, wherein a dramatic increase in reduction of HP [1-^{13}C] DHA in tumors compared with surrounding tissue was confirmed to predominantly reflect increased glutathione (28, 29). Similarly, in a murine model of type 2 diabetes and diabetic nephropathy, wherein overproduction of ROS leads to oxidative stress, a decrease was observed in the reduction of HP [1-^{13}C] DHA in diabetic kidneys,

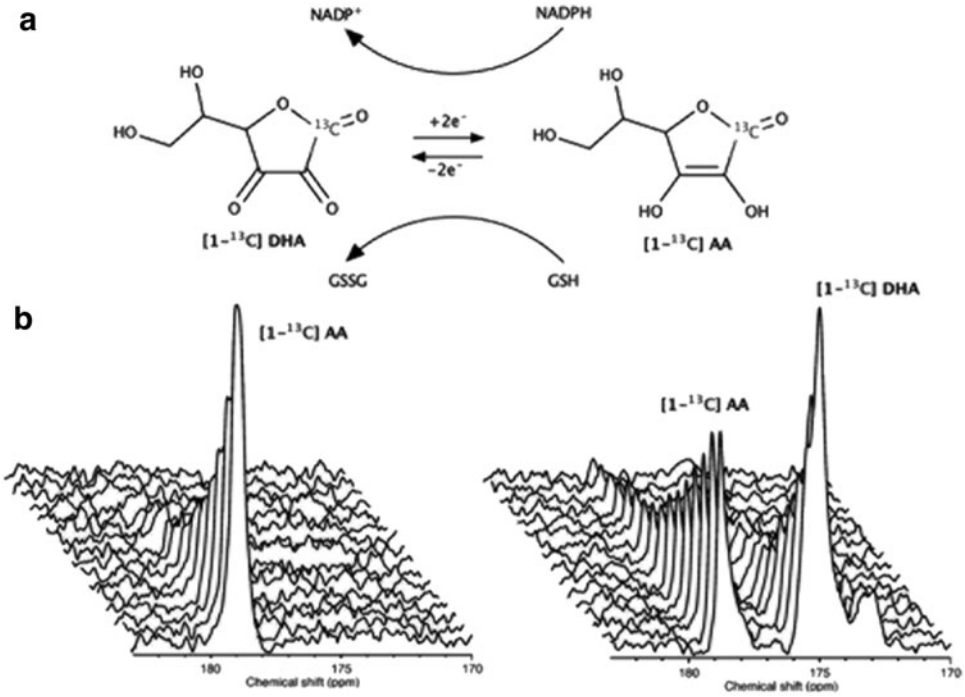

FIG. 3. Probing redox state with HP ^{13}C DHA and AA. **(a)** Schematic of the two-electron reduction of DHA to AA mediated by a GSH or NADPH-dependent mechanism. **(b)** HP ^{13}C MR spectra as a function of time in murine lymphoma tumors after injection of HP [1-^{13}C] AA (*left*) and HP [1-^{13}C] DHA (*right*). Although no HP [1-^{13}C] DHA is generated after injection of HP [1-^{13}C] AA, there is a rapid reduction of HP [1-^{13}C] DHA to HP [1-^{13}C] AA on injection of HP [1-^{13}C] DHA [adapted from Fig. 5 of Bohndiek *et al.* (6)]. AA, ascorbic acid; DHA, dehydroascorbic acid; GSH, glutathione.

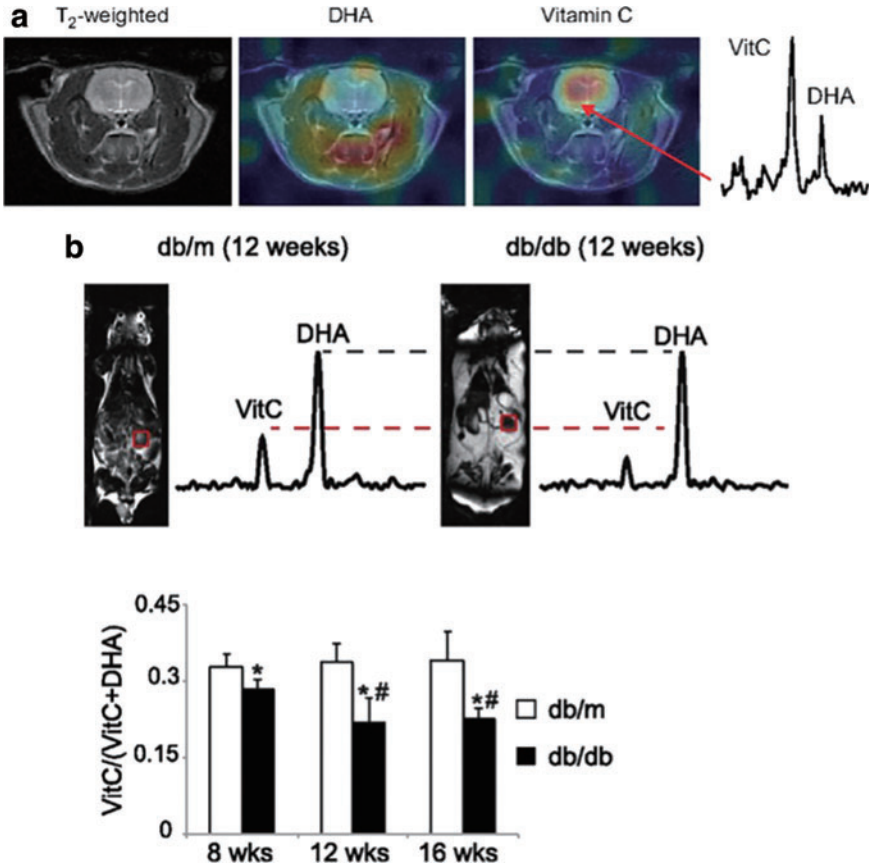

FIG. 4. ***In vivo*** **imaging of redox state with HP ^{13}C DHA and AA (labelled VitC here).** **(a)** T_2-weighted anatomical ^{1}H MR image of a healthy rat head, overlaid with HP [1-^{13}C] DHA and [1-^{13}C] AA signals acquired by using MRSI, in respective *panels*. *Right*: ^{13}C spectrum obtained from the brain region, indicating high levels of HP [1-^{13}C] AA, which reflects the reductive power of the brain [reproduced from Fig. 4 of Keshari *et al.* (28)]. **(b)** ^{13}C spectra acquired from the kidney (localization shown on anatomical ^{1}H MR images) using MRSI in db/db and db/m mice; db/db mice are commonly used as a model of human type 2 diabetes; and db/m are age-matched healthy control mice. A significant decrease in the reduction of HP [1-^{13}C] DHA to [1-^{13}C] AA in the kidney was observed in the db/db mice compared with db/m mice, quantified by the renal AA/(AA+DHA) [VitC/(VitC+DHA)] ratios (*lower panel*) [reproduced from Fig. 2 of Keshari *et al.* (32) with permission from the American Diabetes Association]. ($^*p < 0.05$ when compared with age-matched db/m mice. $^{\#}p < 0.05$ when compared with 8 wks db/db mice.) MRSI, magnetic resonance spectroscopic imaging. Color images are available online.

indicative of reduced GSH concentration (32) (Fig. 4b). The sensitivity of HP [1-^{13}C] DHA is yet to be directly compared with that of alternative MRI redox probes such as nitroxide radicals (27), and it may find application as part of a suite of imaging assessments, including such nitroxides and/or HP [1-^{13}C] pyruvate (43); the possibility of co-polarization with HP [1-^{13}C] pyruvate has yet to be explored.

Beyond DHA-AA metabolism, several other HP ^{13}C-labeled tracers have been studied as potential indicators of redox state. For example, Lewis *et al.* reported that an increase in [1-^{13}C] pyruvate to [1-^{13}C] lactate conversion in the heart on metformin treatment was accompanied by an increase in heart and liver cytosolic redox state, indicating that pyruvate–lactate metabolism is capable of detecting cytoplasmic redox state (Fig. 2c) (39). However, pyruvate–lactate conversion as a measurement of cellular redox state is constrained by [1-^{13}C] pyruvate signal from the vasculature and extra-cellular lactate production; to this end, HP [1-^{13}C] alanine presents an alternative potential tracer of intracellular redox state, where conversion to [1-^{13}C] pyruvate and [1-^{13}C] lactate is indicative of cytosolic [NAD$^+$]/[NADH] levels (55).

More recently, HP [1,3-$^{13}C_2$] Acetoacetate and its reduction to [1,3-$^{13}C_2$] β-hydroxybutyrate have been utilized to directly interrogate mitochondrial redox state in the rat kidney (71) and isolated, perfused rat hearts (10). This conversion is catalyzed by the mitochondrial enzyme β-hydroxybutyrate dehydrogenase and is indicative of the redox state of the NAD(H) system. Metformin treatment was confirmed to increase renal production of HP [1,3-$^{13}C_2$] β-hydroxybutyrate in rats (71), and similar increased production was observed in ischemic rat hearts and those exposed to a complex I inhibitor, when compared with control hearts (10). It is also worth noting that HP ^{13}C-benzoylformic acid has been investigated as a potential tracer with sensitivity to the concentration of hydrogen peroxide (41)—a key metabolite in cellular redox processes; however, *in vivo* application is yet to be reported. HP d-[1,2,3,4,5,6,6-$^{13}C_6$] glucose-d_7 has been utilized to quantify in-cell free cytosolic [NAD$^+$]/[NADH] ratios (11), however *in vivo* application is constrained by the prohibitively low T_1 relaxation time, especially when the molecule is not fully deuterated.

Applications of HP ^{13}C MRI in Various Diseases

Shifts in metabolic flux are a characteristic accompaniment of all pathological conditions, some of which are strongly coupled with tissue redox state especially when the catalytic enzyme requires cofactors such as NAD(H) and can be useful biomarkers to evaluate the extent of the disease and its response to treatments. In this section, we further discuss specific medical conditions for which HP ^{13}C MRI holds particular promise.

Monitoring cancer treatment response

The tumor microenvironment is characterized by chronic and transient hypoxia (45). Upregulation of hypoxia inducible factor signaling evokes a metabolic shift from oxidative phosphorylation (OXPHOS) to glycolysis and generation of a highly reducing redox state in tumors (27). As pyruvate stands at the key branching point of glucose metabolism, HP [1-^{13}C] pyruvate MRI can provide unique information on the OXPHOS-to-glycolysis metabolic shift. As described in the earlier subsections, the feasibility of detection, malignancy assessment, and staging of tumors has been demonstrated in several cancerous organs in humans (21, 51).

Recent research in the field has focused on the monitoring of cancer treatment response. The characteristic aerobic glycolysis in tumors (Warburg effect) is mediated by the activation of mammalian target of rapamycin (mTOR) signaling and cellular Abelson kinase ABL1 regulated oxidative stress in fumarate hydratase-deficient tumor. Inhibition of ABL1 phosphorylation by Vandetanib and resultant alteration of glycolytic tumor metabolism can be readily observed by metabolic MRI of HP [1-^{13}C] pyruvate (65). Further, cancerous cell death is a ubiquitous indicator of tumor treatment response. Monitoring of necrotic cell death using HP [1,4-$^{13}C_2$] fumarate has been reported for treatment-induced cancerous cell death by chemotherapy and photoimmunotherapy (20, 33).

Direct evidence of a correlation between tissue redox state change and metabolism in response to anticancer treatment was investigated with antiangiogenic agent sunitinib treatment of murine tumor xenografts (43). The reduction rate of a redox-sensitive MRI contrast agent 3-carbamoyl-PROXYL was significantly decreased, indicating an oxidative shift in tissue redox potential, 2–4 days after sunitinib treatment during the time known as the vascular re-normalization window (Fig. 5a, b). Consistently, HP [1-^{13}C] pyruvate MRI showed that pyruvate-to-lactate metabolic flux decreased during the same time period, 2–4 days after sunitinib administration (Fig. 5c, d). There is an increasing body of evidence to suggest that metabolic MRI of HP ^{13}C-labeled tracers can provide noninvasive imaging biomarkers of tissue redox state in response to cancer treatments.

Potential applications in heart diseases

The heart pumps 5–6 L of blood every minute and requires a large amount of energy to generate the mechanical force. To fulfill this energy demand, cardiomyocytes are densely packed with mitochondria and consume a large amount of oxygen for OXPHOS. This makes the heart especially susceptible to hypoxia, oxidative stress, and changes in the mitochondrial influx of substrates such as pyruvate. In the following, we consider three specific heart disorders for which HP ^{13}C MRI could have a clinical impact.

Ischemic heart disease is caused by stenosis or occlusion of coronary arteries, leading to hypoxia and dysfunction of the downstream myocardium. Historically, ischemic heart disease was diagnosed by evaluating the degree of coronary stenosis. However, recent evidence suggests that the degree of stenosis does not necessarily correlate with the degree of tissue hypoxia, and thus direct measurement of tissue hypoxia is becoming increasingly important for making treatment decisions (42, 64). The heart mainly uses fatty acid as the substrate for OXPHOS, but during hypoxia, OXPHOS ceases, and glycolysis becomes the primary mode of ATP production. For this reason, FDG-PET imaging, which visualizes the extent of glucose utilization, has been used for detecting cardiac ischemia. However, since glucose can also be oxidized by OXPHOS, ^{18}FDG-PET lacks specificity to glycolysis.

In contrast, HP [1-^{13}C] pyruvate MRI can provide unique information as to whether glucose is being used for OXPHOS

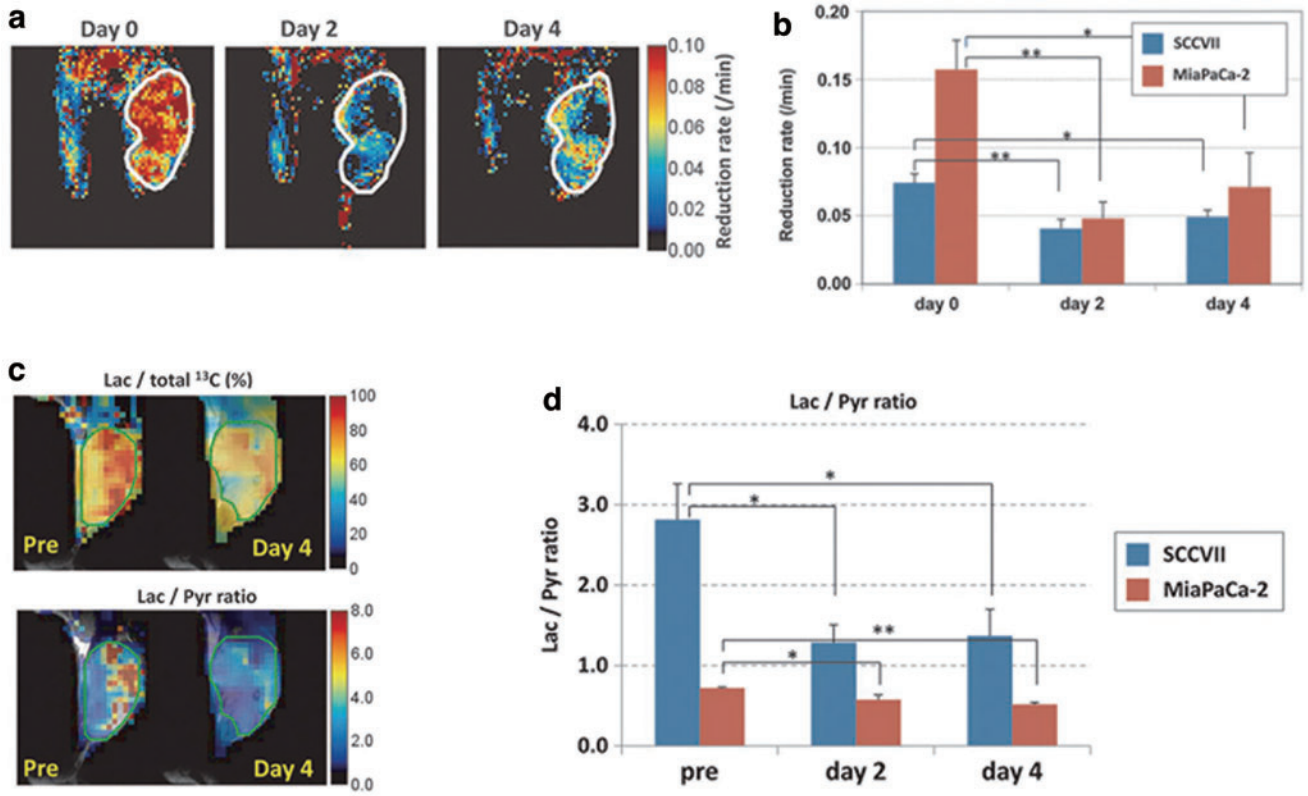

FIG. 5. Effect of treatment with the antiangiogenic agent sunitinib on tumor redox state and HP [1-^{13}C] pyruvate metabolism. **(a)** Reduction rate maps of the redox-sensitive MRI contrast agent 3-carbamoyl-PROXYL in a SCCVII tumor obtained before and after 2 and 4 days of sunitinib treatment. **(b)** Average reduction rate of 3-carbamoyl-PROXYL in SCCVII and MiaPaCa-2 tumor regions. **(c)** Maps of HP ^{13}C lactate-to-total ^{13}C and lactate-to-pyruvate ratios before and 4 days after sunitinib treatment in SCCVII tumors. **(d)** Average HP ^{13}C lactate-to-pyruvate ratio in SCCVII and MiaPaCa-2 tumor regions [reproduced from Figs. 4 and 5 of Matsumoto *et al.* (43)]. $*p<0.05$. $**p<0.01$. MRI, magnetic resonance imaging; SCCVII, murine squamous cell carcinoma cell line. Color images are available online.

or glycolysis by tracking the fate of pyruvate. The HP [1-^{13}C] pyruvate MRI-derived lactate-to-pyruvate ratio within a tissue reflects the NAD^+/NADH ratio and the level of oxidative stress, which builds up during ischemia and thus holds promise for detecting cardiac ischemia. In preclinical cardiac ischemia models, an increase in pyruvate-to-lactate conversion *in vivo* has been reported (49). Further, the technique has recently been proven feasible in humans with a sufficient spatial resolution (Fig. 6a) (15), and further clinical application is anticipated.

Diabetic cardiomyopathy occurs independently of cardiac ischemia in diabetic patients. It is characterized by structural and functional alterations of the heart, such as hypertrophy, fibrosis, diastolic dysfunction, and systolic dysfunction. Although its molecular mechanisms are still under investigation, decreased pyruvate oxidization, excessive fatty oxidization, and increased oxidative stress have been reported as prominent metabolic features of the diabetic heart (53). In a rodent model of diabetic cardiomyopathy, HP [1-^{13}C] pyruvate MRI revealed a decrease in pyruvate oxidation, and treatment was successfully performed by upregulating pyruvate dehydrogenase activity (Fig. 6b) (38). Recently, a similar decrease in cardiac pyruvate oxidation was observed by using HP [1-^{13}C] pyruvate MRI in human diabetic patients with only mild insulin resistance (57), suggesting that the technique is sufficiently sensitive to detect the earliest changes in cardiac metabolism in diabetes. Response to metformin, an anti-diabetic drug and a complex I inhibitor that ameliorates oxidative stress in the heart, can also be monitored with HP [1-^{13}C] pyruvate MRI (39). We anticipate further application of the technique to aid diagnoses, guide treatment, and provide novel insights on the molecular basis of diabetic cardiomyopathy.

Inflammatory heart diseases, such as sarcoidosis and myocarditis, are characterized by excessive inflammation of the myocardium and resulting tissue necrosis. Radioisotope imaging, namely Gallium-67 scintigraphy and ^{18}FDG-PET, are currently used clinically for diagnoses and evaluating response to immunosuppressive therapy. However, periodic appraisal with a short interval, which is especially useful for evaluating treatment response, is difficult due to the ionizing radiation exposure. As HP [1-^{13}C] pyruvate can detect tissue inflammation and HP [1,4-$^{13}C_2$] fumarate can detect cardiac tissue necrosis (40, 47), we anticipate that a combined metabolic MRI protocol with these safe, nonionizing HP tracers could provide a powerful alternative to the current radioisotope-based imaging for treatment optimization.

Inflammation and infections

Excess generation of ROS in inflammatory diseases diminishes the antioxidant capacity of the cell and can induce

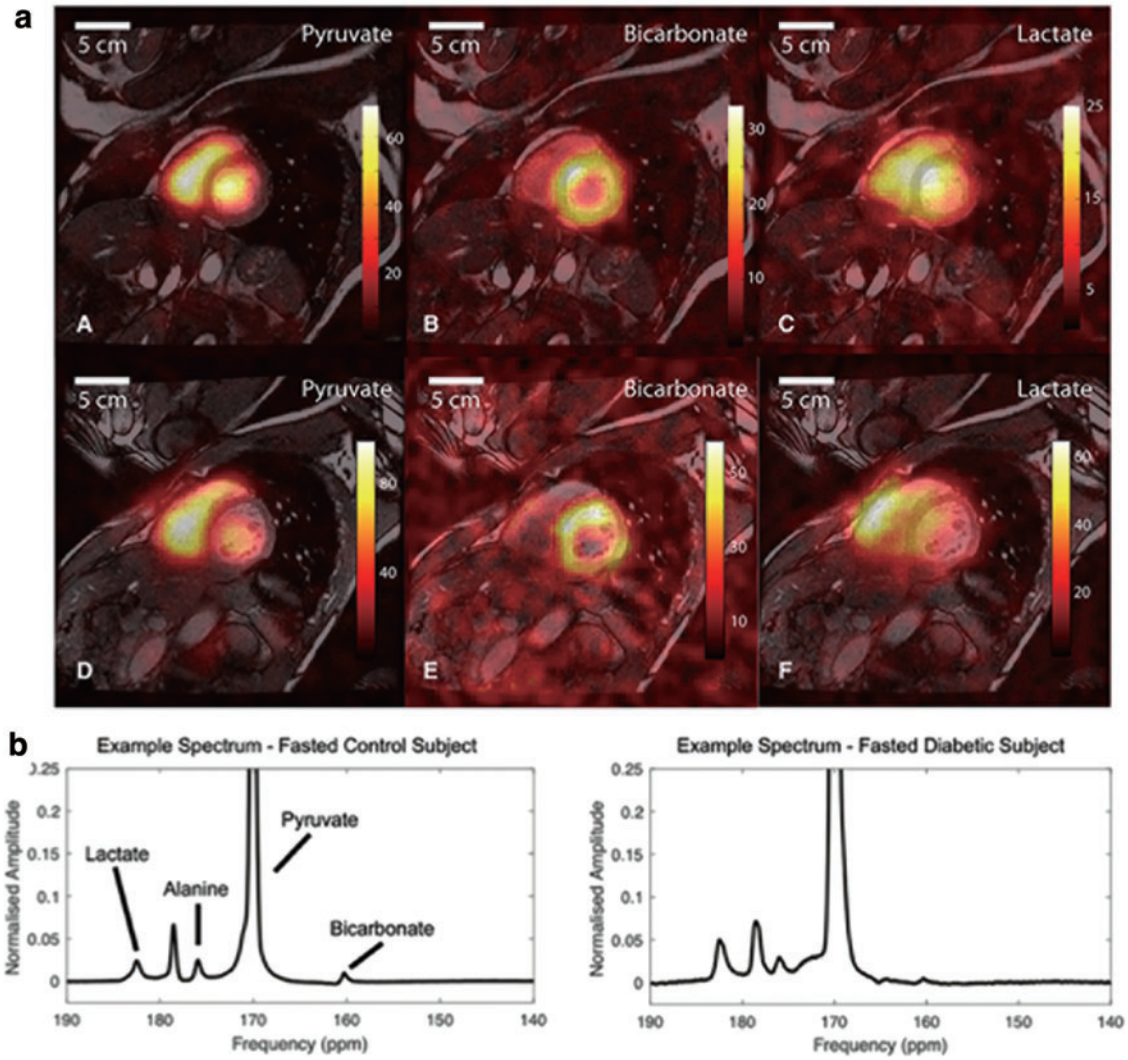

FIG. 6. Imaging cardiac metabolism with HP [1-^{13}C] pyruvate MRI. (a) HP [1-^{13}C] pyruvate MRI of the human heart (two healthy subjects: **A–C** and **D–F**, respectively) *in vivo*, demonstrating clear visualization of pyruvate metabolism with significant spatial resolution [reproduced from Fig. 1 of Cunningham *et al.* (15)]. **(b)** HP ^{13}C MR spectra from healthy and diabetic individuals. HP [1-^{13}C] pyruvate MR spectroscopy clearly depict changes in pyruvate metabolism in the human diabetic heart *in vivo*, *highlighting* reduced bicarbonate production and increased pyruvate–lactate metabolism [reproduced from Fig. 3 of Rider *et al.* (57)]. Color images are available online.

redox-dependent alterations to metabolism. Wilson *et al.* reported that the diminished liver antioxidant capacity in a mouse model of nonalcoholic steatohepatitis can be estimated from the reduction rate of HP [1-^{13}C] DHA to AA (73). As discussed earlier, this conversion is known to occur in a GSH-dependent manner, catalyzed by redox-regulating enzymes, including glutaredoxin and glutathione transferases. The severity of hepatitis can be also evaluated by the extent of cell death using HP ^{13}C fumarate. We recently reported a feasibility study of *in vivo* necrotic cell death imaging in an acetaminophen-induced hepatitis model using HP [1-^{13}C] fumarate, which was prepared by PHIP, a relatively low-cost alternative polarization technique to d-DNP, with a *trans*-selective hydrogenation catalyst (67). Localization of the necrotic cell death biomarkers [1-^{13}C] and [4-^{13}C] malate was observed only at the liver region of hepatitis mice when compared with healthy mice (Fig. 7).

The human coronavirus-2 (HCoV-2), also known as severe acute respiratory syndrome-related coronavirus 2 (SARS-CoV-2), is an enveloped positive-sense and single-stranded RNA virus causative of coronavirus disease (COVID-19) and led to the present global pandemic. The excess activation of the immune system due to viral infection and resultant acute burst of oxidative stress lead to a cytokine storm in COVID-19 patients, similar to Influenza viral infection, and which may lead to multiple organ failure and, ultimately, death. SARS-CoV-2, similar to most of the other viruses, requires host cells to provide the building blocks for viral replication, and it achieves this by rewiring host cell metabolism, including an increase of glucose carbon entry into the TCA cycle *via* pyruvate carboxylase expression, and a decrease in oxidative glutamine metabolism (50). The mTORC1, one of two protein complexes of mTOR, may be involved in the viral infection-induced metabolic alteration. Tarasenko *et al.*

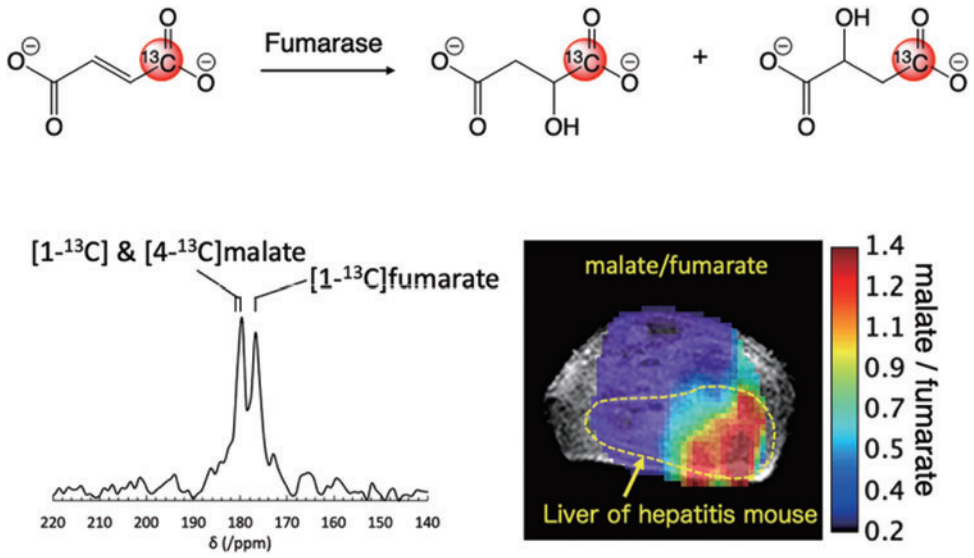

FIG. 7. Feasibility of *in vivo* necrotic cell death imaging using HP [1-^{13}C] fumarate prepared by the PHIP technique with a *trans*-selective hydrogenation catalyst, demonstrated in an acetaminophen-induced hepatitis mouse model [adapted from Fig. 5 of Stewart *et al.* (67)]. PHIP, parahydrogen-induced polarization. Color images are available online.

recently reported that HP ^{13}C MRI of pyruvate metabolism can visualize the mitochondrial metabolic alterations induced by injection with polyinosinic:polycytidylic acid (poly I:C), which chemically mimics RNA virus infection, and that the metabolic alteration was suppressed in mTOR knockout mice (Fig. 8) (69). These reports suggest that HP ^{13}C metabolic MRI of redox-sensitive ^{13}C tracers can provide a useful clinical tool to investigate the underlying mechanism of redox alteration in inflammation and infection, and so establish strategies for therapeutic intervention.

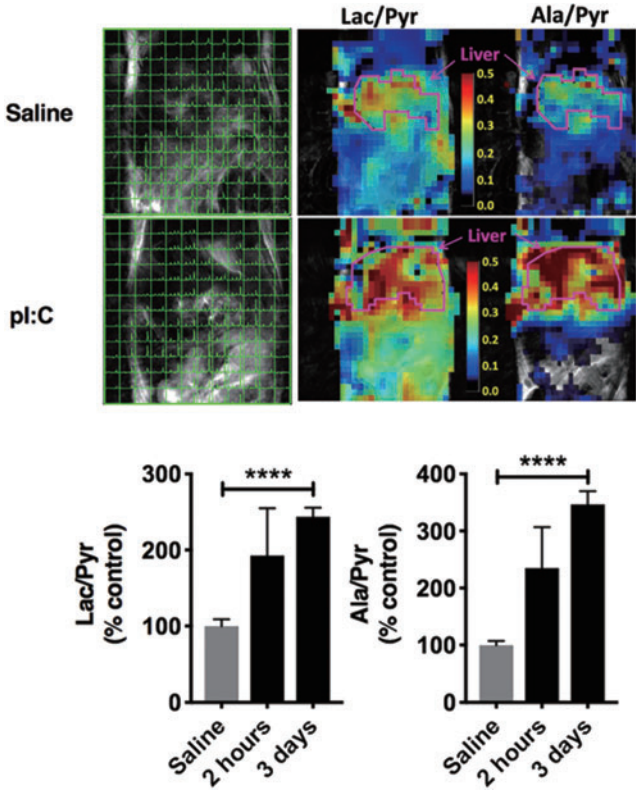

FIG. 8. HP ^{13}C MRI of pyruvate metabolism in a poly I:C-induced mimic model of RNA viral infection. Significant acceleration of the metabolic flux to both lactate and alanine from pyruvate was observed 3 days after poly I:C injection [adapted from Fig. 2 of Tarasenko *et al.* (69) with permission from the Springer Nature]. ****$p < 0.0001$. poly I:C, polyinosinic:polycytidylic acid. Color images are available online.

Future prospects

HP ^{13}C MRI, wherein more than 10,000 times enhancement of the MRI signal of ^{13}C-labeled redox-sensitive metabolic tracers can be realized, has enabled real-time, noninvasive imaging of metabolism *in vivo* and opened new research avenues for the field of redox biology. Although more than 60 ^{13}C metabolic tracers have been reported and attempts have been made at developing specific tracers for detecting ROS (60), to date only a few metabolic tracers have been established for monitoring tissue redox state. As such, future development of new redox-sensitive metabolic tracers and a comprehensive understanding of the correlation between metabolic alterations and the redox state are essential. Recent progress in cost-effective parahydrogen-induced polarization techniques, in addition to conventional d-DNP type methods, may provide a relatively easier entry point for researchers in the redox field to begin HP ^{13}C MRI studies, and additional avenues for novel HP ^{13}C tracer development.

Authors' Contributions

N.T. and T.S. contributed to the writing of the ''Potential applications in heart diseases'' section in this review article. All other sections were written by N.J.S., H.H., and S.M.

Acknowledgments

The authors acknowledge funding support from AMED (Grant No. JP20hm0102061) and the Japan Society for the Promotion of Science (JSPS) KAKENHI (Grant No. 20H006540).

Author Disclosure Statement

No competing financial interests exist.

Funding Information

This research was supported by AMED (Grant No. JP20hm0102061) and the Japan Society for the Promotion of Science (JSPS) KAKENHI (Grant No. 20H006540) to Norihiko Takeda and Shingo Matsumoto.

References

1. Adams RW, Aguilar JA, Atkinson KD, Cowley MJ, Elliott PI, Duckett SB, Green GG, Khazal IG, Lopez-Serrano J, and Williamson DC. Reversible interactions with para-hydrogen enhance NMR sensitivity by polarization transfer. *Science* 323: 1708–1711, 2009.
2. Aggarwal R, Vigneron DB, and Kurhanewicz J. Hyperpolarized 1-[(13)C]-pyruvate magnetic resonance imaging detects an early metabolic response to androgen ablation therapy in prostate cancer. *Eur Urol* 72: 1028–1029, 2017.
3. Albers MJ, Bok R, Chen AP, Cunningham CH, Zierhut ML, Zhang VY, Kohler SJ, Tropp J, Hurd RE, Yen YF, Nelson SJ, Vigneron DB, and Kurhanewicz J. Hyperpolarized 13C lactate, pyruvate, and alanine: noninvasive biomarkers for prostate cancer detection and grading. *Cancer Res* 68: 8607–8615, 2008.
4. Ardenkjaer-Larsen JH, Fridlund B, Gram A, Hansson G, Hansson L, Lerche MH, Servin R, Thaning M, and Golman K. Increase in signal-to-noise ratio of >10,000 times in liquid-state NMR. *Proc Natl Acad Sci U S A* 100: 10158–10163, 2003.
5. Ardenkjaer-Larsen JH, Leach AM, Clarke N, Urbahn J, Anderson D, and Skloss TW. Dynamic nuclear polarization polarizer for sterile use intent. *NMR Biomed* 24: 927–932, 2011.
6. Bohndiek SE, Kettunen MI, Hu DE, Kennedy BW, Boren J, Gallagher FA, and Brindle KM. Hyperpolarized [1-13C]-ascorbic and dehydroascorbic acid: vitamin C as a probe for imaging redox status in vivo. *J Am Chem Soc* 133: 11795–11801, 2011.
7. Bowers CR and Weitekamp DP. Parahydrogen and synthesis allow dramatically enhanced nuclear alignment. *J Am Chem Soc* 109: 5541–5542, 1987.
8. Brender JR, Kishimoto S, Merkle H, Reed G, Hurd RE, Chen AP, Ardenkjaer-Larsen JH, Munasinghe J, Saito K, Seki T, Oshima N, Yamamoto K, Choyke PL, Mitchell J, and Krishna MC. Dynamic imaging of glucose and lactate metabolism by (13)C-MRS without hyperpolarization. *Sci Rep* 9: 3410, 2019.
9. Chattergoon N, Martinez-Santiesteban F, Handler WB, Ardenkjaer-Larsen JH, and Scholl TJ. Field dependence of T1 for hyperpolarized [1-13C]pyruvate. *Contrast Media Mol Imaging* 8: 57–62, 2013.
10. Chen W, Sharma G, Jiang W, Maptue NR, Malloy CR, Sherry AD, and Khemtong C. Metabolism of hyperpolarized (13) C-acetoacetate to beta-hydroxybutyrate detects real-time mitochondrial redox state and dysfunction in heart tissue. *NMR Biomed* 32: e4091, 2019.
11. Christensen CE, Karlsson M, Winther JR, Jensen PR, and Lerche MH. Non-invasive in-cell determination of free cytosolic [NAD+]/[NADH] ratios using hyperpolarized glucose show large variations in metabolic phenotypes. *J Biol Chem* 289: 2344–2352, 2014.
12. Chung BT, Chen HY, Gordon J, Mammoli D, Sriram R, Autry AW, Le Page LM, Chaumeil MM, Shin P, Slater J, Tan CT, Suszczynski C, Chang S, Li Y, Bok RA, Ronen SM, Larson PEZ, Kurhanewicz J, and Vigneron DB. First hyperpolarized [2-(13)C]pyruvate MR studies of human brain metabolism. *J Magn Reson* 309: 106617, 2019.
13. Coffey AM, Shchepin RV, Truong ML, Wilkens K, Pham W, and Chekmenev EY. Open-source automated para-hydrogen hyperpolarizer for molecular imaging using (13)C metabolic contrast agents. *Anal Chem* 88: 8279–8288, 2016.
14. Cortese-Krott MM, Koning A, Kuhnle GGC, Nagy P, Bianco CL, Pasch A, Wink DA, Fukuto JM, Jackson AA, van Goor H, Olson KR, and Feelisch M. The reactive species interactome: evolutionary emergence, biological significance, and opportunities for redox metabolomics and personalized medicine. *Antioxid Redox Signal* 27: 684–712, 2017.
15. Cunningham CH, Lau JY, Chen AP, Geraghty BJ, Perks WJ, Roifman I, Wright GA, and Connelly KA. Hyperpolarized 13C metabolic MRI of the human heart: initial experience. *Circ Res* 119: 1177–1182, 2016.
16. Day SE, Kettunen MI, Gallagher FA, Hu DE, Lerche M, Wolber J, Golman K, Ardenkjaer-Larsen JH, and Brindle KM. Detecting tumor response to treatment using hyperpolarized 13C magnetic resonance imaging and spectroscopy. *Nat Med* 13: 1382–1387, 2007.
17. Drachman N, Kadlecek S, Pourfathi M, Xin Y, Profka H, and Rizi R. In vivo pH mapping of injured lungs using hyperpolarized [1-(13) C]pyruvate. *Magn Reson Med* 78: 1121–1130, 2017.
18. Eigenberg R. Parahydrogen-induced polarization: a new spin on reactions with molecular hydrogen. *Acc Chem Res* 24: 110–116, 1991.
19. Gallagher FA, Kettunen MI, Day SE, Hu DE, Ardenkjaer-Larsen JH, Zandt R, Jensen PR, Karlsson M, Golman K, Lerche MH, and Brindle KM. Magnetic resonance imaging of pH in vivo using hyperpolarized 13C-labelled bicarbonate. *Nature* 453: 940–943, 2008.
20. Gallagher FA, Kettunen MI, Hu DE, Jensen PR, Zandt RI, Karlsson M, Gisselsson A, Nelson SK, Witney TH, Bohndiek SE, Hansson G, Peitersen T, Lerche MH, and Brindle KM. Production of hyperpolarized [1,4-13C2]malate from [1,4-13C2]fumarate is a marker of cell necrosis and treatment response in tumors. *Proc Natl Acad Sci U S A* 106: 19801–19806, 2009.
21. Gallagher FA, Woitek R, McLean MA, Gill AB, Manzano Garcia R, Provenzano E, Riemer F, Kaggie J, Chhabra A, Ursprung S, Grist JT, Daniels CJ, Zaccagna F, Laurent MC, Locke M, Hilborne S, Frary A, Torheim T, Boursnell C, Schiller A, Patterson I, Slough R, Carmo B, Kane J, Biggs H, Harrison E, Deen SS, Patterson A, Lanz T, Kingsbury Z, Ross M, Basu B, Baird R, Lomas DJ, Sala E, Wason J, Rueda OM, Chin SF, Wilkinson IB, Graves MJ, Abraham JE, Gilbert FJ, Caldas C, and Brindle KM. Imaging breast cancer using hyperpolarized carbon-13 MRI. *Proc Natl Acad Sci U S A* 117: 2092–2098, 2020.
22. Golman K, Zandt RI, Lerche M, Pehrson R, and Ardenkjaer-Larsen JH. Metabolic imaging by hyperpolarized 13C magnetic resonance imaging for in vivo tumor diagnosis. *Cancer Res* 66: 10855–10860, 2006.
23. Grist JT, McLean MA, Riemer F, Schulte RF, Deen SS, Zaccagna F, Woitek R, Daniels CJ, Kaggie JD, Matys T, Patterson I, Slough R, Gill AB, Chhabra A, Eichenberger R, Laurent MC, Comment A, Gillard JH, Coles AJ, Tyler DJ, Wilkinson I, Basu B, Lomas DJ, Graves MJ, Brindle KM, and Gallagher FA. Quantifying normal human brain

metabolism using hyperpolarized [1-(13)C]pyruvate and magnetic resonance imaging. *Neuroimage* 189: 171–179, 2019.
24. Gudbjarnason S and Bing RJ. The redox-potential of the lactate-pyruvate system in blood as an indicator of the functional state of cellular oxidation. *Biochim Biophys Acta* 60: 158–162, 1962.
25. Harrison C, Yang C, Jindal A, DeBerardinis RJ, Hooshyar MA, Merritt M, Dean Sherry A, and Malloy CR. Comparison of kinetic models for analysis of pyruvate-to-lactate exchange by hyperpolarized 13 C NMR. *NMR Biomed* 25: 1286–1294, 2012.
26. Hu S, Yoshihara HA, Bok R, Zhou J, Zhu M, Kurhanewicz J, and Vigneron DB. Use of hyperpolarized [1-13C]pyruvate and [2-13C]pyruvate to probe the effects of the anticancer agent dichloroacetate on mitochondrial metabolism in vivo in the normal rat. *Magn Reson Imaging* 30: 1367–1372, 2012.
27. Hyodo F, Matsumoto K, Matsumoto A, Mitchell JB, and Krishna MC. Probing the intracellular redox status of tumors with magnetic resonance imaging and redox-sensitive contrast agents. *Cancer Res* 66: 9921–9928, 2006.
28. Keshari KR, Kurhanewicz J, Bok R, Larson PE, Vigneron DB, and Wilson DM. Hyperpolarized 13C dehydroascorbate as an endogenous redox sensor for in vivo metabolic imaging. *Proc Natl Acad Sci U S A* 108: 18606–18611, 2011.
29. Keshari KR, Sai V, Wang ZJ, Vanbrocklin HF, Kurhanewicz J, and Wilson DM. Hyperpolarized [1-13C]dehydroascorbate MR spectroscopy in a murine model of prostate cancer: comparison with 18F-FDG PET. *J Nucl Med* 54: 922–928, 2013.
30. Keshari KR, Sriram R, Koelsch BL, Van Criekinge M, Wilson DM, Kurhanewicz J, and Wang ZJ. Hyperpolarized 13C-pyruvate magnetic resonance reveals rapid lactate export in metastatic renal cell carcinomas. *Cancer Res* 73: 529–538, 2013.
31. Keshari KR and Wilson DM. Chemistry and biochemistry of 13C hyperpolarized magnetic resonance using dynamic nuclear polarization. *Chem Soc Rev* 43: 1627–1659, 2014.
32. Keshari KR, Wilson DM, Sai V, Bok R, Jen KY, Larson P, Van Criekinge M, Kurhanewicz J, and Wang ZJ. Noninvasive in vivo imaging of diabetes-induced renal oxidative stress and response to therapy using hyperpolarized 13C dehydroascorbate magnetic resonance. *Diabetes* 64: 344–352, 2015.
33. Kishimoto S, Oshima N, Yamamoto K, Munasinghe J, Ardenkjaer-Larsen JH, Mitchell JB, Choyke PL, and Krishna MC. Molecular imaging of tumor photoimmunotherapy: evidence of photosensitized tumor necrosis and hemodynamic changes. *Free Radic Biol Med* 116: 1–10, 2018.
34. Kohler SJ, Yen Y, Wolber J, Chen AP, Albers MJ, Bok R, Zhang V, Tropp J, Nelson S, Vigneron DB, Kurhanewicz J, and Hurd RE. In vivo 13 carbon metabolic imaging at 3T with hyperpolarized 13C-1-pyruvate. *Magn Reson Med* 58: 65–69, 2007.
35. Larson PE, Bok R, Kerr AB, Lustig M, Hu S, Chen AP, Nelson SJ, Pauly JM, Kurhanewicz J, and Vigneron DB. Investigation of tumor hyperpolarized [1–13C]-pyruvate dynamics using time-resolved multiband RF excitation echo-planar MRSI. *Magn Reson Med* 63: 582–591, 2010.
36. Lau AZ, Miller JJ, Robson MD, and Tyler DJ. Simultaneous assessment of cardiac metabolism and perfusion using copolarized [1-(13) C]pyruvate and (13) C-urea. *Magn Reson Med* 77: 151–158, 2017.
37. Laustsen C, Nielsen PM, Qi H, Lobner MH, Palmfeldt J, and Bertelsen LB. Hyperpolarized [1,4-(13)C]fumarate imaging detects microvascular complications and hypoxia mediated cell death in diabetic nephropathy. *Sci Rep* 10: 9650, 2020.
38. Le Page LM, Rider OJ, Lewis AJ, Ball V, Clarke K, Johansson E, Carr CA, Heather LC, and Tyler DJ. Increasing pyruvate dehydrogenase flux as a treatment for diabetic cardiomyopathy: a combined 13C hyperpolarized magnetic resonance and echocardiography study. *Diabetes* 64: 2735–2743, 2015.
39. Lewis AJ, Miller JJ, McCallum C, Rider OJ, Neubauer S, Heather LC, and Tyler DJ. Assessment of metformin-induced changes in cardiac and hepatic redox state using hyperpolarized[1-13C]pyruvate. *Diabetes* 65: 3544–3551, 2016.
40. Lewis AJM, Miller JJ, Lau AZ, Curtis MK, Rider OJ, Choudhury RP, Neubauer S, Cunningham CH, Carr CA, and Tyler DJ. Noninvasive immunometabolic cardiac inflammation imaging using hyperpolarized magnetic resonance. *Circ Res* 122: 1084–1093, 2018.
41. Lippert AR, Keshari KR, Kurhanewicz J, and Chang CJ. A hydrogen peroxide-responsive hyperpolarized 13C MRI contrast agent. *J Am Chem Soc* 133: 3776–3779, 2011.
42. Maron DJ, Hochman JS, Reynolds HR, Bangalore S, O'Brien SM, Boden WE, Chaitman BR, Senior R, Lopez-Sendon J, Alexander KP, Lopes RD, Shaw LJ, Berger JS, Newman JD, Sidhu MS, Goodman SG, Ruzyllo W, Gosselin G, Maggioni AP, White HD, Bhargava B, Min JK, Mancini GBJ, Berman DS, Picard MH, Kwong RY, Ali ZA, Mark DB, Spertus JA, Krishnan MN, Elghamaz A, Moorthy N, Hueb WA, Demkow M, Mavromatis K, Bockeria O, Peteiro J, Miller TD, Szwed H, Doerr R, Keltai M, Selvanayagam JB, Steg PG, Held C, Kohsaka S, Mavromichalis S, Kirby R, Jeffries NO, Harrell FE, Jr., Rockhold FW, Broderick S, Ferguson TB, Jr., Williams DO, Harrington RA, Stone GW, Rosenberg Y; ISCHEMIA Research Group. Initial Invasive or Conservative Strategy for Stable Coronary Disease. *N Engl J Med* 382: 1395–1407, 2020.
43. Matsumoto S, Saito K, Takakusagi Y, Matsuo M, Munasinghe JP, Morris HD, Lizak MJ, Merkle H, Yasukawa K, Devasahayam N, Suburamanian S, Mitchell JB, and Krishna MC. In vivo imaging of tumor physiological, metabolic, and redox changes in response to the anti-angiogenic agent sunitinib: longitudinal assessment to identify transient vascular renormalization. *Antioxid Redox Signal* 21: 1145–1155, 2014.
44. Matsumoto S, Saito K, Yasui H, Morris HD, Munasinghe JP, Lizak M, Merkle H, Ardenkjaer-Larsen JH, Choudhuri R, Devasahayam N, Subramanian S, Koretsky AP, Mitchell JB, and Krishna MC. EPR oxygen imaging and hyperpolarized 13C MRI of pyruvate metabolism as noninvasive biomarkers of tumor treatment response to a glycolysis inhibitor 3-bromopyruvate. *Magn Reson Med* 69: 1443–1450, 2013.
45. Matsumoto S, Yasui H, Mitchell JB, and Krishna MC. Imaging cycling tumor hypoxia. *Cancer Res* 70: 10019–10023, 2010.

46. Milani J, Vuichoud B, Bornet A, Mieville P, Mottier R, Jannin S, and Bodenhausen G. A magnetic tunnel to shelter hyperpolarized fluids. *Rev Sci Instrum* 86: 024101, 2015.
47. Miller JJ, Lau AZ, Nielsen PM, McMullen-Klein G, Lewis AJ, Jespersen NR, Ball V, Gallagher FA, Carr CA, Laustsen C, Botker HE, Tyler DJ, and Schroeder MA. Hyperpolarized [1,4-(13)C2]fumarate enables magnetic resonance-based imaging of myocardial necrosis. *JACC Cardiovasc Imaging* 11: 1594–1606, 2018.
48. Miloushev VZ, Granlund KL, Boltyanskiy R, Lyashchenko SK, DeAngelis LM, Mellinghoff IK, Brennan CW, Tabar V, Yang TJ, Holodny AI, Sosa RE, Guo YW, Chen AP, Tropp J, Robb F, and Keshari KR. Metabolic imaging of the human brain with hyperpolarized (13)C pyruvate demonstrates (13)C lactate production in brain tumor patients. *Cancer Res* 78: 3755–3760, 2018.
49. Moon CM, Kim YH, Ahn YK, Jeong MH, and Jeong GW. Metabolic alterations in acute myocardial ischemia-reperfusion injury and necrosis using in vivo hyperpolarized [1-(13)C] pyruvate MR spectroscopy. *Sci Rep* 9: 18427, 2019.
50. Mullen PJ, Garcia G, Jr., Purkayastha A, Matulionis N, Schmid EW, Momcilovic M, Sen C, Langerman J, Ramaiah A, Shackelford DB, Damoiseaux R, French SW, Plath K, Gomperts BN, Arumugaswami V, and Christofk HR. SARS-CoV-2 infection rewires host cell metabolism and is potentially susceptible to mTORC1 inhibition. *Nat Commun* 12: 1876, 2021.
51. Nelson SJ, Kurhanewicz J, Vigneron DB, Larson PE, Harzstark AL, Ferrone M, van Criekinge M, Chang JW, Bok R, Park I, Reed G, Carvajal L, Small EJ, Munster P, Weinberg VK, Ardenkjaer-Larsen JH, Chen AP, Hurd RE, Odegardstuen LI, Robb FJ, Tropp J, and Murray JA. Metabolic imaging of patients with prostate cancer using hyperpolarized [1-(1)(3)C]pyruvate. *Sci Transl Med* 5: 198ra108, 2013.
52. Ostergaard Mariager C, Nielsen PM, Qi H, Schroeder M, Bertelsen LB, and Laustsen C. Can hyperpolarized (13)C-urea be used to assess glomerular filtration rate? A retrospective study. *Tomography* 3: 146–152, 2017.
53. Palomer X, Pizarro-Delgado J, and Vazquez-Carrera M. Emerging actors in diabetic cardiomyopathy: heartbreaker biomarkers or therapeutic targets? *Trends Pharmacol Sci* 39: 452–467, 2018.
54. Park I, Bok R, Ozawa T, Phillips JJ, James CD, Vigneron DB, Ronen SM, and Nelson SJ. Detection of early response to temozolomide treatment in brain tumors using hyperpolarized 13C MR metabolic imaging. *J Magn Reson Imaging* 33: 1284–1290, 2011.
55. Park JM, Khemtong C, Liu SC, Hurd RE, and Spielman DM. In vivo assessment of intracellular redox state in rat liver using hyperpolarized [1-(13) C]Alanine. *Magn Reson Med* 77: 1741–1748, 2017.
56. Pravica MG and Weitekamp DP. Net NMR alignment by adiabatic transport of parahydrogen addition products to high magnetic field. *Chem Phys Lett* 145: 255–258, 1988.
57. Rider OJ, Apps A, Miller J, Lau JYC, Lewis AJM, Peterzan MA, Dodd MS, Lau AZ, Trumper C, Gallagher FA, Grist JT, Brindle KM, Neubauer S, and Tyler DJ. Noninvasive in vivo assessment of cardiac metabolism in the healthy and diabetic human heart using hyperpolarized (13)C MRI. *Circ Res* 126: 725–736, 2020.
58. Ross B, Lin A, Harris K, Bhattacharya P, and Schweinsburg B. Clinical experience with 13C MRS in vivo. *NMR Biomed* 16: 358–369, 2003.
59. Saito K, Matsumoto S, Takakusagi Y, Matsuo M, Morris HD, Lizak MJ, Munasinghe JP, Devasahayam N, Subramanian S, Mitchell JB, and Krishna MC. 13C-MR spectroscopic imaging with hyperpolarized [1-13C]pyruvate detects early response to radiotherapy in SCC tumors and HT-29 tumors. *Clin Cancer Res* 21: 5073–5081, 2015.
60. Saito K, Sail D, Yamamoto K, Matsumoto S, Blackman B, Kishimoto S, Brender JR, Swenson RE, Mitchell JB, and Krishna MC. Synthesis and evaluation of (13)C-labeled 5-5-dimethyl-1-pyrroline-N-oxide aimed at in vivo detection of reactive oxygen species using hyperpolarized (13)C-MRI. *Free Radic Biol Med* 131: 18–26, 2019.
61. Salamanca-Cardona L and Keshari KR. (13)C-labeled biochemical probes for the study of cancer metabolism with dynamic nuclear polarization-enhanced magnetic resonance imaging. *Cancer Metab* 3: 9, 2015.
62. Schafer FQ and Buettner GR. Redox environment of the cell as viewed through the redox state of the glutathione disulfide/glutathione couple. *Free Radic Biol Med* 30: 1191–1212, 2001.
63. Schroeder MA, Swietach P, Atherton HJ, Gallagher FA, Lee P, Radda GK, Clarke K, and Tyler DJ. Measuring intracellular pH in the heart using hyperpolarized carbon dioxide and bicarbonate: a 13C and 31P magnetic resonance spectroscopy study. *Cardiovasc Res* 86: 82–91, 2010.
64. Shaw LJ, Berman DS, Maron DJ, Mancini GB, Hayes SW, Hartigan PM, Weintraub WS, O'Rourke RA, Dada M, Spertus JA, Chaitman BR, Friedman J, Slomka P, Heller GV, Germano G, Gosselin G, Berger P, Kostuk WJ, Schwartz RG, Knudtson M, Veledar E, Bates ER, McCallister B, Teo KK, Boden WE; COURAGE Investigators. Optimal medical therapy with or without percutaneous coronary intervention to reduce ischemic burden: results from the Clinical Outcomes Utilizing Revascularization and Aggressive Drug Evaluation (COURAGE) trial nuclear substudy. *Circulation* 117: 1283–1291, 2008.
65. Sourbier C, Ricketts CJ, Matsumoto S, Crooks DR, Liao PJ, Mannes PZ, Yang Y, Wei MH, Srivastava G, Ghosh S, Chen V, Vocke CD, Merino M, Srinivasan R, Krishna MC, Mitchell JB, Pendergast AM, Rouault TA, Neckers L, and Linehan WM. Targeting ABL1-mediated oxidative stress adaptation in fumarate hydratase-deficient cancer. *Cancer Cell* 26: 840–850, 2014.
66. Stewart NJ and Matsumoto S. Biomedical applications of the dynamic nuclear polarization and parahydrogen induced polarization techniques for hyperpolarized (13)C MR imaging. *Magn Reson Med Sci* 20: 1–17, 2021.
67. Stewart NJ, Nakano H, Sugai S, Tomohiro M, Kase Y, Uchio Y, Yamaguchi T, Matsuo Y, Naganuma T, Takeda N, Nishimura I, Hirata H, Hashimoto T, and Matsumoto S. Hyperpolarized 13C MRI of fumarate metabolism by parahydrogen-induced polarization: a proof-of-concept in vivo study. *Chemphyschem* 22: 915–923, 2021.
68. Stodkilde-Jorgensen H, Laustsen C, Hansen ESS, Schulte R, Ardenkjaer-Larsen JH, Comment A, Frokiaer J, Ringgaard S, Bertelsen LB, Ladekarl M, and Weber B. Pilot study experiences with hyperpolarized [1-(13) C]pyruvate

MRI in pancreatic cancer patients. *J Magn Reson Imaging* 51: 961–963, 2020.
69. Tarasenko TN, Jestin M, Matsumoto S, Saito K, Hwang S, Gavrilova O, Trivedi N, Zerfas PM, Barca E, DiMauro S, Senac J, Venditti CP, Cherukuri M, and McGuire PJ. Macrophage derived TNFalpha promotes hepatic reprogramming to Warburg-like metabolism. *J Mol Med (Berl)* 97: 1231–1243, 2019.
70. von Morze C, Larson PE, Hu S, Keshari K, Wilson DM, Ardenkjaer-Larsen JH, Goga A, Bok R, Kurhanewicz J, and Vigneron DB. Imaging of blood flow using hyperpolarized [(13)C]urea in preclinical cancer models. *J Magn Reson Imaging* 33: 692–697, 2011.
71. von Morze C, Ohliger MA, Marco-Rius I, Wilson DM, Flavell RR, Pearce D, Vigneron DB, Kurhanewicz J, and Wang ZJ. Direct assessment of renal mitochondrial redox state using hyperpolarized (13) C-acetoacetate. *Magn Reson Med* 79: 1862–1869, 2018.
72. Wiesinger F, Weidl E, Menzel MI, Janich MA, Khegai O, Glaser SJ, Haase A, Schwaiger M, and Schulte RF. IDEAL spiral CSI for dynamic metabolic MR imaging of hyperpolarized [1-13C]pyruvate. *Magn Reson Med* 68: 8–16, 2012.
73. Wilson DM, Di Gialleonardo V, Wang ZJ, Carroll V, Von Morze C, Taylor A, Sai V, VanCriekinge M, Bok R, Ohliger MA, and Keshari KR. Hyperpolarized (13)C spectroscopic evaluation of oxidative stress in a rodent model of steatohepatitis. *Sci Rep* 7: 46014, 2017.
74. Witney TH, Kettunen MI, Hu DE, Gallagher FA, Bohndiek SE, Napolitano R, and Brindle KM. Detecting treatment response in a model of human breast adenocarcinoma using hyperpolarised [1-13C]pyruvate and [1,4-13C2]fumarate. *Br J Cancer* 103: 1400–1406, 2010.
75. Woitek R, McLean MA, Gill AB, Grist JT, Provenzano E, Patterson AJ, Ursprung S, Torheim T, Zaccagna F, Locke M, Laurent MC, Hilborne S, Frary A, Beer L, Rundo L, Patterson I, Slough R, Kane J, Biggs H, Harrison E, Lanz T, Basu B, Baird R, Sala E, Graves MJ, Gilbert FJ, Abraham JE, Caldas C, Brindle KM, and Gallagher FA. Hyperpolarized (13)C MRI of tumor metabolism demonstrates early metabolic response to neoadjuvant chemotherapy in breast cancer. *Radiol Imaging Cancer* 2: e200017, 2020.

Address correspondence to:
Dr. Shingo Matsumoto
Division of Bioengineering & Bioinformatics
Graduate School of Information Science & Technology
Hokkaido University
North 14, West 9, Kita-ku
Sapporo 060-0814
Japan

E-mail: smatsumoto@ist.hokudai.ac.jp

Date of first submission to ARS Central, June 26, 2021; date of acceptance, June 29, 2021.

Abbreviations Used

AA = ascorbic acid
ADME = absorption, distribution, metabolism and excretion
d-DNP = dissolution dynamic nuclear polarization
DHA = dehydroascorbic acid
FDG-PET = fluorodeoxyglucose-positron emission tomography
GSH = glutathione
HCoV-2 = human coronavirus-2
HP = hyperpolarized/hyperpolarization
LDH = lactate dehydrogenase
MR = magnetic resonance
MRI = magnetic resonance imaging
MRSI = magnetic resonance spectroscopic imaging
mTOR = mammalian target of rapamycin
NMR = nuclear magnetic resonance
OXPHOS = oxidative phosphorylation
PHIP = parahydrogen-induced polarization
poly I:C = polyinosinic:polycytidylic acid
ROS = reactive oxygen species
SARS-CoV-2 = severe acute respiratory syndrome-related coronavirus 2
SCCVII = murine squamous cell carcinoma cell line
TRAMP = transgenic adenocarcinoma of the mouse prostate